

# Design of CMOS Avalanche Photodiode for Embedded Laser Range Finder

Irfan Abdul Bari  
Stud. Dept. of ECE,  
Shadan college of engineering and Technology  
Hyderabad, India

Prof. Abdul Mubeen  
Dept. of ECE  
Shadan college of engineering and Technology  
Hyderabad, India

## Abstract

*In this paper, the design of CMOSAPD in standard 0.35  $\mu\text{m}$  CMOS technology is presented; Simulation and Comparison between two CMOS avalanche photodiode (APDs) modes are performed. Electrical and Optical Simulations are carried out using SILVACO ATLAS<sup>®</sup> Suite. Two modes of Electrical Simulation have been presented. The performances of APDs in both modes have been compared in terms of responsivity, noise and gain. Both structures present interesting characteristics. Monolithic integration of sensors and circuits in CMOS processes result in tremendous advantages in terms of dimensions shrink, low power consumption, low cost etc.*

**Keywords**— CMOS APD, Range Finder, SPAD, Distance measurement, integrated Optoelectronics.

## I. INTRODUCTION

Avalanche photodiodes (APDs) are very attractive devices for their high sensitivity in low light level and even high speed applications such as long distance, optical communications and optical distance measurement. APDs have been well known for decades, but high reverse voltage needed to allow avalanche mechanism in the multiplication region prevented their fabrication in standard CMOS technology.

Avalanche photodiode (APD) is the keystone of the accurate embedded system for distance measurement, thanks to a strong internal gain and a high bandwidth. However, there are two main difficulties to take into account when designing a CMOS APD. First, the realization of the APD has to be compatible with the CMOS process characteristics. Second, the APD has to operate with a sufficient voltage, allowing for avalanche mode without destroying the device, particularly at the peripheral junction. The usually used solution is the implementation of a guard ring [1] that generally consists in a slightly doped region at the peripheral junction because a slightly doped region holds tension better than a heavily doped one.

The Avalanche process occurs when the carriers in the transition region are accelerated by the

electric field to energies sufficient to free e-h pairs via collisions with bond electrons. An Avalanche diode is a diode (usually made from silicon, but can be made from another semiconductor) that is designed to go through avalanche breakdown at a specified reverse bias voltage and conduct as a type of voltage reference.

Some CMOS APDs have been previously reported. Most of them are developed for photon counter applications in Geiger mode [2,3,4]. They are implemented in CMOS technologies at  $< 0.2 \mu\text{m}$ , and the guard rings are realized with a p-well. Some of them have a buried n-type isolation layer that prevents a punchthrough of the p-well guard ring to the P-substrate. Moreover, CMOS APDs working as an optoelectronic mixer have been also reported for fiber-supported wireless systems [5]. Here, the guard ring is implemented by a shallow trench isolation (STI). The problem when using STI is that it may dramatically increase the density of deep-level carrier generation centers at its interface, which strongly increases the dark current. In all the cases, the major objective is to work at high frequencies but not to optimize the sensitivity. That is the reason why the surfaces are small ( $< 900 \mu\text{m}^2$ ), the working wavelengths are high (between 600 and 800 nm), and the APDs operate very near the breakdown in order to minimize the junction capacity.

The rest of the paper is organized as follows: Section II presents Laser range Finder. Section III, presents the design of CMOS APD in 0.35 $\mu\text{m}$  tech. Section IV presents the results and discussion. Section V presents the electrical and optical simulations performed. Finally, section VI draws some conclusion.

**II. LASER RANGE FINDER**

Time-of-flight laser range-finding methods are commonly used for Range-Finding applications and can be divided into three categories: pulsed technique, phase-shifting measurement, and frequency modulation continuous wave method [6, 7, 8]. These techniques are based on the time-of-flight measurement of a laser beam and consist in measuring the transit time of the light to reach any diffusing target and return. In the case of using a phase-shifting method, the dc current of an emitting laser diode (LD) is modulated by a sine wave generated by a reference oscillator at the frequency  $f_{rf}$ . After reflection from the diffusing surface of the target, a part of the laser beam is collected by a photodiode through a focusing lens. Distance measurement  $D$  is deduced from the phase shift  $\Delta\phi$  existing between the photoelectric current and the modulated laser signal, as follows (Eqn. 1), where  $c$  is the speed of light and  $\tau_d$  is the time of flight:

$$\Delta\phi = 2\pi f_{rf} \frac{2 \cdot D}{c} = 2 \cdot \pi \cdot f_{rf} \cdot \tau_d(1)$$

The distance resolution  $\delta D$  is determined by the Equation 2 using phase-shift resolution  $\delta\phi$ .

$$\delta D = (2) \quad 1 / (2 \cdot \pi \cdot f_{rf}) \cdot c / 2 \cdot \delta\phi$$

Then, the sensitivity  $SD$  is deduced from Equation 3 given below:

$$S_D = \delta D / \delta\phi = 1 / (2 \cdot \pi \cdot f_{rf}) \cdot c / 2(3)$$

The maximum measurement range  $\Lambda$  is then

$$\Lambda = c / 2f_{rf}(4)$$

Hence, this method allows one to obtain a high distance resolution if the modulation frequency  $f_{rf}$  is high. To facilitate phase measurement, the

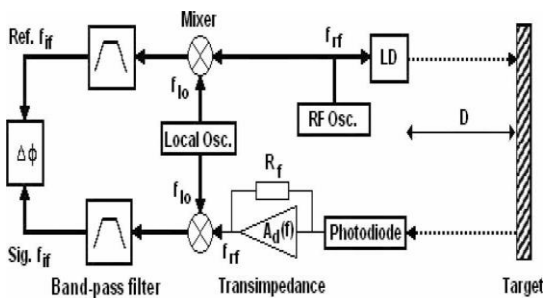


**Fig. 1 Phase-shift rangefinder with electronic heterodyne technique setup.**

photoelectric signal and the oscillator signal frequencies are both reduced by using an electronic heterodyne technique. (Fig. 1)

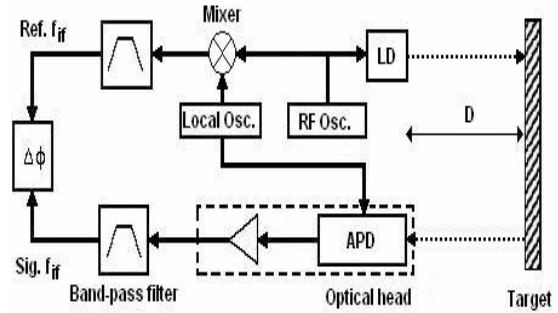


**Fig. 2 Phase-shift rangefinder with optoelectronic heterodyne technique setup.**

The photoelectric signal is mixed with a signal given by a balanced modulator whose frequency  $f_{lo}$  is close to  $f_{rf}$ . This heterodyne detection gives a better phase measurement resolution without changing the phase shift [9].

The major drawbacks of the electronic heterodyne technique are crosstalk effects between emitting and receiving circuits and a low signal-to-noise ratio (SNR). This is due to the low open loop gain  $Ad(f)$  of the transimpedance amplifier which works at high frequencies ( $f_{rf}$ ). To improve the SNR and to minimize the crosstalk effects, one could perform optoelectronic mixing through an APD. With this technique, shown in Fig. 2, the frequency of the useful signal received by the transimpedance amplifier is  $f_{if}$ , which strongly reduces the noise equivalent bandwidth. A supply voltage, in general, on the order of some hundreds of volts, in the case of commercial APD, is needed to apply an electric field important enough to release an avalanche in the multiplication region. Such a value of supply voltage is incompatible with embedded systems. Hence, it would be interesting to integrate an APD in a conventional CMOS technology to realize optoelectronic mixing in the case of a low-noise, low-consumption, compact, and accurate embedded rangefinder. Aside from this, the possibility of implementing the APD, together with the preamplifier circuit, could minimize the parasitic capacitors so as to still improve the bandwidth and the SNR.

**III. DESIGN OF CMOS AVALANCHE PHOTODIODE**

An APD is designed in AMS 0.35- $\mu\text{m}$  CMOS technology after the optimization of its performances with SILVACO. The highest possible conversion gain is expected, as well as an avalanche voltage as low as possible. 0.35 $\mu\text{m}$  technology specs.

The main characteristics of the AMS CMOS 0.35- $\mu\text{m}$  technology are reported in Table 1. The weak depths and the high doping values can be pointed out.

**Table 1 Main characteristics of the AMS CMOS 0.35- $\mu\text{m}$  technology**

Layer	Doping ( $\text{cm}^{-3}$ )	Depth ( $\mu\text{m}$ )
Substrate P	$1,25 \cdot 10^{15}$	-
N Well	$1,28 \cdot 10^{17}$	1,2
P Well	$2,00 \cdot 10^{17}$	1,2
Contact N+	$5,00 \cdot 10^{19}$	0,2
Contact P+	$5,00 \cdot 10^{19}$	0,2

Note that the small interval  $d$  separating both n-wells is smaller than the minimum value allowed by the AMS design rules. Finally, the guard ring is constituted by a weakly doped N-ring due to the n-wells lateral diffusion, whose geometry is not optimum but sufficiently decreases the breakdown voltage of the peripheral junction.

A cross-sectional view is shown in Fig 3. In CMOS technology, the multiplication of the photo generated carriers is realized in the absorption area, a very thin region where the electrical field is maximal. It is therefore impossible to separate the absorption area of the photons and the multiplication region of the carriers. The conception of this structure consists principally in taking into account two main difficulties. The first one concerns the technological constraints imposed by AMS. The main characteristics of the AMS CMOS 0.35- $\mu\text{m}$  technology are reported in Table 1. The weak depths and the high doping values can be pointed out.

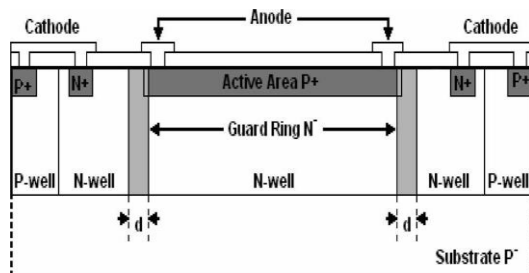


**Fig. 3 Cross-section view of the CMOS APD developed with a guard ring.**

The second difficulty is avoiding the early breakdown of the P<sup>+</sup>N peripheral junction due to the higher electrical field at the peripheral junction than at the planar junction.

**IV. RESULTS AND DISCUSSION**

The spectral responsivity  $S_{\lambda\text{APD}}$  (in amperes per watt) of the APD has been measured by comparing the photoelectric current of the APD with the one obtained by a commercial photodiode PIN

(BPW34) whose  $S_{\lambda\text{PIN}}$  values are well known (4). The results obtained are reported in Fig. 4

$$S_{\lambda\text{APD}} = \frac{I_{\text{phAPD}}}{P_{\text{opt}}} = \frac{I_{\text{phAPD}}}{I_{\text{phPIN}}} \cdot \frac{A_{\text{PIN}}}{A_{\text{APD}}} \cdot S_{\lambda\text{PIN}} \quad (5)$$

With  $A_{\text{APD}}$  and  $A_{\text{PIN}}$ , respectively, as the active areas of the studied APD and the reference PIN and with  $I_{\text{phPIN}}$  and  $I_{\text{phAPD}}$ , respectively, as the photocurrents of the reference photodetector and the APD.  $P_{\text{opt}}$  is theoptical power received by both photodiodes.

A better responsivity is obtained for short wavelengths. This is due to the penetration depth of

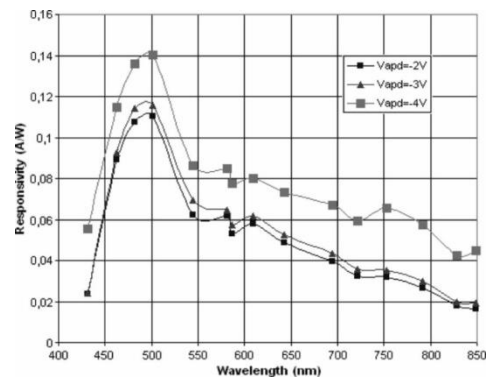


**Fig. 4 Spectral responsivity  $S_{\lambda\text{APD}}$  of CMOS APD for different reverse voltages.**

photons in the device. In fact, the ideal photon penetration depth is equal to the P<sup>+</sup> layer depth (0.1  $\mu\text{m}$ ) plus the depletion region depth (0.13  $\mu\text{m}$  at -1V).

**Table 2 Absorption Rate for Several Wavelengths.**

$\lambda$ (nm)	$a$ ( $\text{cm}^{-1}$ )	Absorption rate (%)
650	4625	19
560	15668	39.8
450	32581	74.4

Based on Table 2, the absorption rate of photons in an absorption depth of  $0.28 \mu\text{m}$  with  $\lambda = 450 \text{ nm}$  is around 74%, whereas with  $\lambda = 650 \text{ nm}$ , the photons absorption rate is around 22%. The junction depth is the limiting factor of the integrated APD for working with high wavelengths.

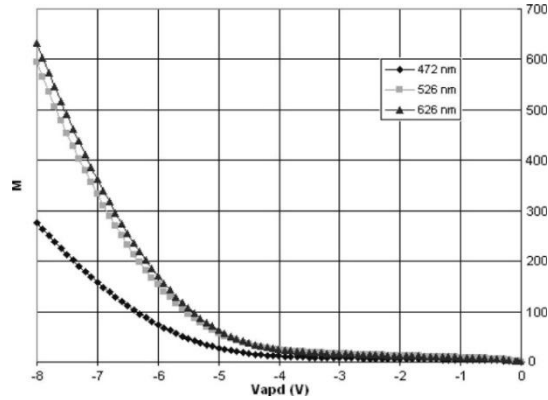


Fig. 5 Internal gain  $M$  versus reverse voltage.

The internal gain  $M$  of the APD is shown in Fig. 5. Note that better values of the internal gain are obtained for the largest wavelengths; however, these are not interesting because the absorption coefficient (as well as the responsivity) decreases strongly with the wavelength, reducing the SNR. When biased at  $-6 \text{ V}$ , the APD has an internal gain of about 75 at  $\lambda = 450 \text{ nm}$ .

Finally, the APD is designed in an optoelectronic mixer in the rangefinder, with  $f_{rf} = 1 \text{ MHz}$ . This low frequency gives a measurement range  $\Lambda = 150 \text{ m}$  and a distance resolution  $\delta D = 4.2 \text{ cm}$ . The rangefinder can thus be easily embedded in a vehicle for an obstacle-detection application, where this low resolution is sufficient.

## V. SIMULATION RESULTS

Electrical and optical simulations presented in this section have been performed using ATLAS<sup>®</sup> Software.

### A. P<sup>+</sup>N Structure

The first simulation concerns the electrical field in the structure to ensure the efficiency of the guard ring. The horizontal distribution is reported in Fig. 6. At a reverse bias voltage of  $-5 \text{ volts}$ , the maximum horizontal electrical field at the peripheral junction is about  $2.901 \text{ V.cm}^{-1}$ . In the same condition, the vertical electrical field is about  $7.552 \text{ V.cm}^{-1}$ . The electrical field is stronger vertically in the multiplication region than horizontally at the peripheral junction.

Then the spectral responsivity of the device has been studied and presented in Fig. 7. It presents a

maximum around  $450 \text{ nm}$ . The simulation is performed for  $V_{\text{apd}} = -1 \text{ V}$  not to be in avalanche mode. At this reverse bias value, the depletion region depth is equal to  $0.355 \mu\text{m}$ . Table 2 represents the absorption rate according to the wavelength. One can easily notice that  $\alpha$  greatly increases for short wavelengths. That is why a cut-off of the photoresponse can be observed in short wavelengths range. The photons are essentially absorbed very close to the surface, where the recombination time is extremely short.

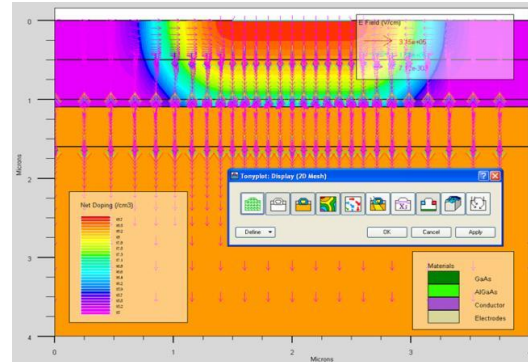


Fig. 6 Cross section of the P+N photodiode: Horizontal Electrical field distribution.

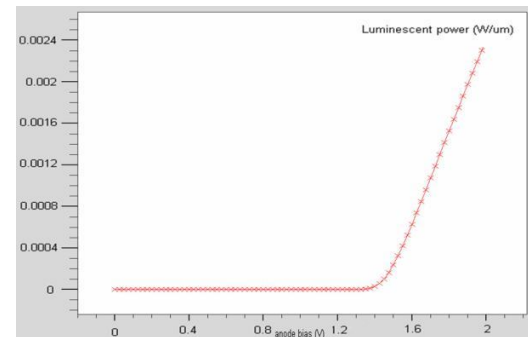


Fig 7. Photodiode responsivity according to the wavelength of the incident light beam.

The photoelectric gain  $M$  has also been evaluated at the best responsivity  $\lambda = 450 \text{ nm}$ . In the middle of the non-linear region, i.e. for a reverse bias voltage  $V_{\text{apd}} = -5 \text{ V}$ ,  $M = 55$ .

### B. N<sup>+</sup>P Structure

The study of the electrical field in this structure has brought us to determine the best structure with the suitable gap width  $d$ . The best structure is obtained for a gap width of  $1 \mu\text{m}$ . The vertical electrical field distribution is reported in Fig. 8 When reverse biased at  $-5 \text{ volts}$ , the maximum horizontal electrical field at the peripheral junction is about  $7.985 \text{ V.cm}^{-1}$ . In the same condition, the vertical electrical field is about  $0.905 \text{ V.cm}^{-1}$ . The chosen guard ring is efficient and decreases efficiently the electrical field at the

peripheral junction.

The spectral responsivity of the N<sup>+</sup>P avalanche photodiode is presented in Fig. 9; the maximum is around 350 nm. In this case, a better responsivity is obtained for short wavelengths [6]. This is due to the absorption depth of photons in the device which is thinner than the P<sup>+</sup>N one. At -1 volt, the depletion region depth is equal to 0.082 μm.

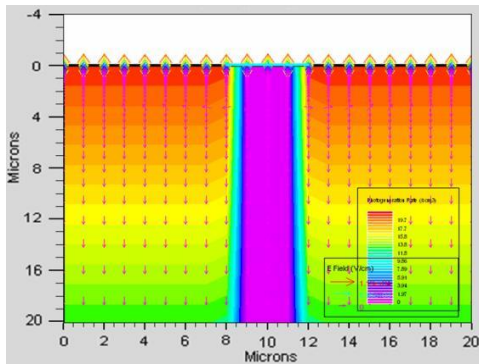


Fig. 8 Cross section of the N<sup>+</sup>P photodiode: vertical electrical field distribution.

At the best responsivity  $\lambda = 550$  nm, in the middle of the nonlinear region, i.e. for a reverse bias voltage  $V_{\text{apd}} = -5$  V, the photoelectric gain  $M = 97$ . The P<sup>+</sup>N APD presents the best responsivity with a peak around 600 nm.

The N<sup>+</sup>P APD presents a peak of responsivity around 475 nm. At the opposite, the excess noise factor is better for the N<sup>+</sup>P structure. Finally, when biased at -6V and for  $\lambda = 475$  nm the photoelectric gain of the N<sup>+</sup>P structure is equal to 100 whereas the P<sup>+</sup>N structure one is equal to 60 at  $\lambda = 650$  nm.

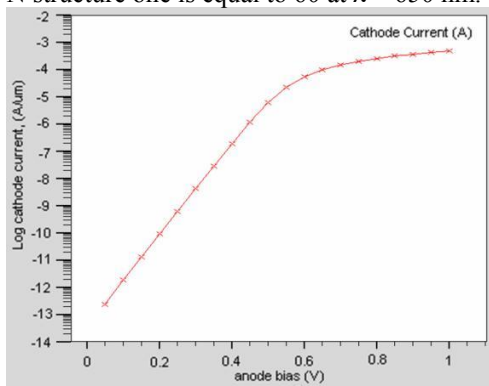


Fig. 9 N<sup>+</sup>P Photodiode responsivity.

## VI. CONCLUSION

In this paper, the feasibility of performing optoelectronic mixing with a CMOS APD is presented and discussed. The use of an APD as an optoelectronic

mixer leads to an improvement of the SNR in a laser phase-shift rangefinder and to a decrease in crosstalk. The CMOS APD developed operates at -5 V, which is compatible with an embedded system. Its ability to realize optoelectronic mixing has been validated at a low frequency ( $f_{\text{rf}} = 1$  MHz) which is suitable for an obstacle-detection application.

This paper presents the conception and simulation of avalanche photodiodes Designed in a standard 0.35 μm CMOS technology. Two designs have been presented, a P<sup>+</sup>N device with a P-tub as guard ring and a N<sup>+</sup>P one with a lateral diffusion of two P-tubs as guard ring. The performances of both devices have been compared in terms of responsivity, noise and gain. The optical simulations present a good responsivity in the short wavelengths. Both structures present interesting characteristics.

The future of this presented work is to conceive a CMOS array composed of a linear or matrix arrangement of APDs to be designed in a 3-D-camera, each APD being individually designed in the CMOS ASIC. This configuration will permit one to work at higher frequencies ( $f_{\text{rf}} = 40$  MHz) in order to significantly improve the resolution ( $\delta D = 1$  mm). A 3-D camera in the range 0.5–5 m, using a PIN photodiode, has already been developed.

For robotic applications, the scanning system must be of small size and as fast as possible. Hence, the laser beam is deflected by two micro-mirrors. Further work includes the design of a scanner-less camera.

## REFERENCES

- [1] Rochas, A. Pauchard, P. A. Besse, D. Pantic, Z. Prijic, and R. S. Popovic, "Low-noise silicon avalanche photodiode s fabricated in conventional CMOS technologies," *IEEE Trans. Electron Devices*, vol. 49, no. 3, pp. 387–394, Mar. 2002.
- [2] C. J. Stapels, W. G. Lawrence, F. L. Augustine, and J. F. Christian, "Characterization of a CMOS Geiger photo diode pixel," *IEEE Trans. Electron Devices*, vol. 53, no. 4, pp. 631–635, Apr. 2006.
- [3] N. Faramazpour, M. Jamal Deen, S. Shirani, and Q. Fang, "Fully integrated single photon avalanche diode detector in standard CMOS 0.18 μm technology," *IEEE Trans. Electron Devices*, vol. 55, no. 3, pp. 760–767, Mar. 2008.
- [4] C. Nicllass, M. Gersbach, R. Henderson, L. Grant, and E. Charbon, "A single photon avalanche diode implement ed in 130-nm CMOS technology," *IEEE J. Sel. Topics Quantum Electron.*, vol. 13, no. 4, pp. 863–869, Jul./Aug. 2007.
- [5] H.-S. Kang and W.-Y. Choi, "Fibre-supported 60 GHz self-heterodyne systems based on CMOS-compatible harmonic optoelectronic mixers," *Electron. Lett.*, vol. 43, no. 20, pp. 1101–1103, Sep. 2007.
- [6] H. Ailisto, V. Heikinen, R. Mitikka, R. Myllyla, J. Kostamovaara, A. Mantyniemi, and M. Koskinen, "Scannerless imaging pulsed-laser range finding," *J. Opt. A, Pure Appl. Opt.*, vol. 4, no. 6, pp. 337–346, Nov. 2002.
- [8] S. Poujouly and B. Journet, "Laser range finding by phase-shift measurement: Moving towards smart systems," in *Proc. SPIE Mach. Vis. Three-Dimensional Imaging Syst. Inspection*

- Metrology*, Boston, MA, vol. 4189, pp. 152–160, Nov. 2000.
- [9] B. Journet and G. Bazin, "A low-cost laser range finder based on an FMCW-like method," *IEEE Trans. Instrum. Meas.*, vol. 49, no. 4, pp. 840–843, Aug. 2000.
- [10] D. Castagnet, H. Tap-Beteille, and M. Lescure, "APD-based heterodyne optical head of a phase-shift laser rangefinder," *Opt. Eng.*, vol. 40, no. 4, pp. 43 003-1–43 003-7, 2006